FLOW TOPOLOGY IN A SQUARE ANNULAR DUCT

Stuart McIlwain
Department of Mechanical Engineering
Queen's Univesity
Kingston, ON, CANADA K7L 3N6

Hongyi Xu
Institute for Aerospace Research
National Research Council
Ottawa, ON, CANADA K1A 0R6

Andrew Pollard
Department of Mechanical Engineering
Queen's Univesity
Kingston, ON, CANADA K7L 3N6

ABSTRACT

Flow topology techniques are applied to a large eddy simulation database of a square annular duct. The helicity density as well as the topology of the eddying motions are calculated as a function of time over the region of flow surrounding one of the inner duct corners. Turbulence structures are identified from the resulting isosurface plots. The structures are formed along the inner wall near the corner, and then transported diagonally away from the inner duct where they are stretched in the downstream direction by the mean flow field.

1. INTRODUCTION

Turbulence structures in a confined flow ought to be affected by the geometry of the enclosure. In the case of a square annular duct (see Figure 1), the evolution of the turbulence structures in the vicinity of the sharp corners of the inner duct will be significantly different from that in other areas of the flow field. The purpose of this study is to investigate how and where turbulence structures are formed along the inner walls of a square annular duct. It is expected that the presence of sharp outside corners of the inner duct will cause the flow field to be significantly different from that of a square duct without an annulus. Structures generated on the outer surface of the inner duct will be transported by the secondary flow patterns towards the corners of the outer duct. The effect of the mean velocity field will be significant, causing the structures to be transported in the downstream direction as well; thus the turbulence structures will be three-dimensional in nature.

A square annular duct was investigated by Xu and Pollard (1997) using a temporal large eddy simulation. They observed strong counter-rotating vortex pairs

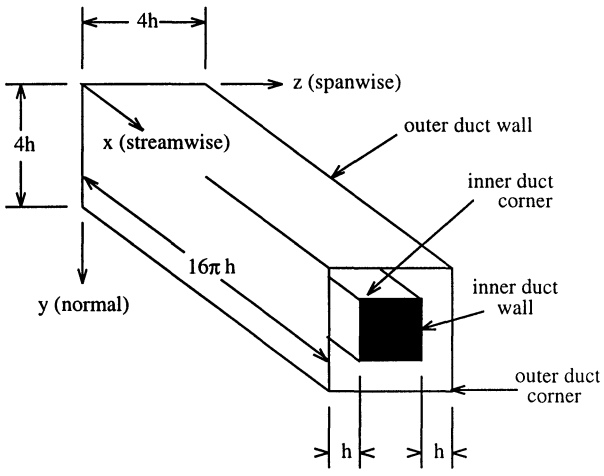

Figure 1: Square annular duct

close to the walls of the inner duct by using the time-averaged velocity and vorticity quantities obtained from the simulation. While time-averaged data do provide useful information about the overall behaviour of the flow field, instantaneous data must also be examined in order to trace the development of turbulence structures. In the present study, flow topology techniques are used to examine the instantaneous quantities from the Xu and Pollard database to determine how the presence of a sharp inner corner affects the turbulent flow field. This includes an examination of the helicity density of the flow field, as well as the topology of the eddying motions as described by Chong *et al.* (1998).

2. NUMERICAL SIMULATION

The Xu and Pollard database was created from a large eddy simulation of a temporally-evolving incompressible turbulent flow in a square annular duct. In a large eddy simulation, the large turbulence motions of the flow are directly calculated, while the smaller motions are modelled through a subgrid scale model to obtain a turbulent viscosity, ν_t. A large eddy simulation uses the following forms of the continuity and Navier-Stokes equations:

$$\frac{\partial u_i}{\partial x_i} = 0 \tag{1}$$

and

$$\frac{\partial u_i}{\partial t} + \frac{\partial u_i u_j}{\partial x_j} = -\frac{\partial p}{\partial x_i} + \frac{1}{Re_\tau}\frac{\partial}{\partial x_j}\left[(1+\nu_t)\left(\frac{\partial u_i}{\partial x_j} + \frac{\partial u_j}{\partial x_i}\right)\right] \tag{2}$$

where u_i are the components of the velocity vector in the x_i direction, corresponding to the x, y, and z coordinates.

The dimensions of the modelled duct were normalized by the half the width of the inner annulus, h. The outer duct was $4h \times 4h$ wide in the normal (y) and spanwise (z) directions, and $16\pi h$ long in the streamwise (x) direction. The Reynolds number of the flow, based upon the frictional velocity, was $Re_\tau = 200$. A fractional step method proposed by Kim *et al.* (1985) was used to achieve velocity-pressure coupling with a second-order accurate time advancement scheme. The timestep used in the simulation, normalised by $h/\overline{U_\tau}$ where $\overline{U_\tau}$ is the mean frictional velocity, was 5×10^{-4}, which maintains a CFL number below 0.5. The equations were discretized in space using a second-order finite volume method. Approximately 400,000 control volumes were used on a non-uniform grid. Initial conditions were constructed from a fully developed laminar velocity profile upon which disturbances that are solutions to the Orr-Sommerfeld equations were imposed. Complete details of the computations can be found in Xu and Pollard (1997).

In the Xu and Pollard database, the Smagorinsky subgrid scale model was used to model the turbulent viscosity,

$$\nu_t = Re_\tau (C_s D_{fcn} \Delta)^2 (2 S_{ij} S_{ij})^{0.5} \tag{3}$$

where Δ is the average cell size, S_{ij} is the symmetric rate of strain tensor, and the Smagorinsky constant $C_s = 0.10$. The Smagorinsky model does not provide for damping of the larger scales of turbulence motion in the near-wall region of flows; thus a damping co-efficient D_{fcn} must be introduced. For the square annular duct simulation, the van Driest wall damping function was applied in two dimensions,

$$D_{fcn} = \left[1 - exp\left(-\frac{y^+}{25}\right)\right]\left[1 - exp\left(-\frac{z^+}{25}\right)\right] \tag{4}$$

where y^+ and z^+ are the distances from the nearest wall, in wall units. The Smagorinsky model has been used fairly successfully to predict the behaviour of turbulent flows having low Reynolds numbers. This may be due to its ability to predict the global energy transfer adequately even if the local transfer is incorrect, Piomelli (1993). Therefore, the mean quantities reported by Xu and Pollard should be reliable. However, the shape of the instantaneous flow structures examined here using flow topology techniques may not be completely accurate.

3. FLOW TOPOLOGY

3.1 Helicity Density

The helicity, H, is defined as the dot product between the velocity and vorticity vectors,

$$H = \overline{V} \cdot \overline{\Omega} \tag{5}$$

where $\overline{\Omega}$ is the vorticity defined by $\overline{\Omega} = \nabla \times \overline{V}$, see Moffat (1969). It is a measure of the transport of vorticity by the velocity field; that is, the movement of the the flow structures downstream in a screw sense. The quantity may be either positive or negative, depending on the orientation of the vectors. The quantity examined in the present study has been normalised

$$H = \frac{\overline{V} \cdot \overline{\Omega}}{|\,\overline{V}\,||\,\overline{\Omega}\,|} \tag{6}$$

to yield a helicity density.

3.2 Topology of Eddying Motions

The geometry of the streamline pattern close to any point in the flow can be classified by studying certain invariants of the velocity gradient tensor, $A_{ij} = \partial u_i / \partial x_j$, at that point, Chong *et al.* (1998). The characteristic equation of A_{ij} is

$$\lambda^3 + P\lambda^2 + Q\lambda + R = 0 \tag{7}$$

where λ represents the eigenvalues, and P, Q, and R are the tensor invarients,

$$P = -tr(\mathbf{A}) \tag{8}$$

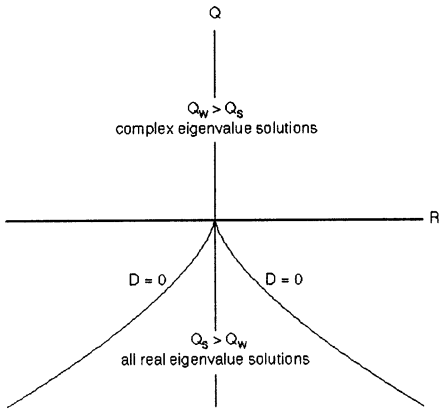

Figure 2: Discriminant $D = 0$ separating regions of $Q - R$ space with complex solutions to the characteristic Equation 7 from those with all real solutions

$$Q = \frac{1}{2}(P^2 - tr(\mathbf{A^2})) \tag{9}$$

and

$$R = -det(\mathbf{A}) \tag{10}$$

For incompressible flow, $P = 0$. The discriminant, D, which describes the surface that divides flows with complex eigenvalues from those with all real eigenvalues is, Chong *et al.* (1990)

$$D = \frac{27}{4}R^2 + Q^3 \tag{11}$$

For regions of the flow where $D > 0$, the characteristic equation admits two complex and one real solution for λ, and the point is classified as a focal region. When $D < 0$, the solutions to the characteristic equation are all real, and the associated pattern is referred to as a node-saddle-saddle point. A plot of $Q - R$ space and the location of the line $D = 0$ is given in Figure 2.

It is possible to obtain a physical understanding of $Q - R$ space by splitting the velocity gradient tensor into two components, Chong *et al.* (1990):

$$A_{ij} = S_{ij} + W_{ij} \tag{12}$$

where S_{ij} is the symmetric rate of strain tensor and W_{ij} is the skew symmetric rate of rotation tensor. These are given by

$$S_{ij} = \frac{1}{2}\left(\frac{\partial u_i}{\partial x_j} + \frac{\partial u_j}{\partial x_i}\right) \tag{13}$$

and

$$W_{ij} = \frac{1}{2}\left(\frac{\partial u_i}{\partial x_j} - \frac{\partial u_j}{\partial x_i}\right) \tag{14}$$

The invariants of S_{ij} (P_S, Q_S, and R_S) and W_{ij} (P_W, Q_W, and R_W) can be defined in an analogous way to the invariants of A_{ij}. For incompressible flow,

$$Q_S = -\frac{1}{2}S_{ij}S_{ij} \tag{15}$$

and

$$Q_W = \frac{1}{2}W_{ij}W_{ij} \tag{16}$$

Thus, Q_W must always be positive; Q_S must always be negative. It can be shown that

$$Q = Q_W + Q_S = \frac{1}{2}(W_{ij}W_{ij} - S_{ij}S_{ij}) \tag{17}$$

Therefore, areas of the flow where the rate of strain tensor is dominated by the rate of rotation tensor ($Q_W > Q_S$) correspond to positive values of Q in $Q - R$ space, or locations where the velocity gradient tensor A_{ij} has complex eigenvalues, Chong *et al.* (1990). Thus, isosurfaces of constant positive D in the flow field enclose concentrated bundles of vortex lines. Areas of the flow where $Q_S > Q_W$ correspond to negative values of D. Turbulence structures, when defined as vorticies in which the rate of rotation tensor dominates the rate of strain tensor, can be identified from plots of isosurfaces of constant positive values of D. Blackburn *et al.* (1996) found that plots of isosurfaces of constant D were superior to plots of isosurfaces of enstrophy density or dissipation of kinetic energy for isolating clear, well-defined structures.

Chong *et al.* (1998) and Blackburn *et al.* (1996) have applied this method to the databases obtained from several direct numerical simulations. However, it is important to note that the results to be presented in the present study are limited due to the coarse resolution of the computational grid from the large eddy simulation compared to that of direct numerical simulations.

4. PRESENTATION AND DISCUSSION OF RESULTS

Three-dimensional plots showing isosurfaces of flow topology features for the entire flow field result in a large number of features which are difficult to interpret. To simplify the plots, only the portion of the flow filed described by ($7.7\pi < x < 8.7\pi$; $0.67 < y < 1.30$; $0.67 < z < 1.30$) is presented here. This corresponds to the region of flow surrounding the top left corner of the inner duct shown in Figure 1. The grid resolution in this portion of the flow domain is $8 \times 16 \times 16$ control volumes. For the flow topology analysis, a total of 100 plots were examined at every 10 timesteps between 39.0 and 39.5 non-dimensional time units into the large eddy simulation. Data from two instances in time are presented here, and are representative of the data observed throughout this time period.

The secondary velocity pattern observed by Xu and Pollard is reproduced in Figure 3 for the region of flow surrounding the upper left corner of the inner duct. Here, the velocity data have been averaged both in time

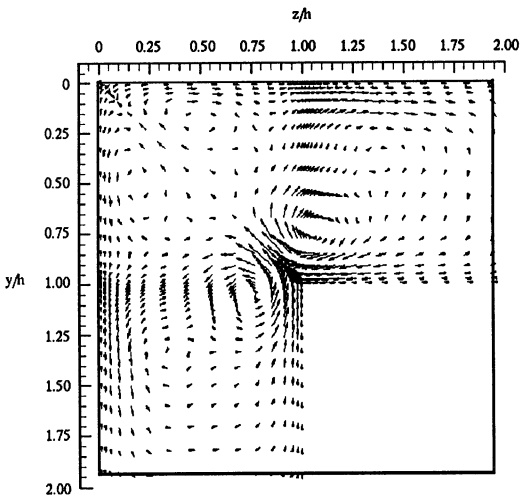

Figure 3: Time-average secondary flow vectors at the inner corner of a square annular duct

and in the x direction. The vorticies next to the inner duct accelerate fluid along the wall towards the corner, and then diagonally out away from the inner duct. The same flow pattern is evident at all four corners.

Isosurface plots of helicity density at 39.175 and 39.230 non-dimensional time units into the large eddy simulation are shown in Figures 4 and 5, respectively. The inner duct is located in the bottom right corners of these plots. The downstream direction of the mean flow field is out of the paper towards the viewer. The regions of flow with the greatest absolute values of helicity density are negative, corresponding to flow with a clockwise rotation. This agrees with the direction of rotation of the vorticies shown in Figure 3. The helicity density plots highlight turbulence structures, corresponding to areas of high vorticity and hence high absolute helicity density, being transported downstream with time. One such structure, labelled Structure 2, can be observed at the top of Figure 4, mid-way along the x-axis. In Figure 5, the same structure has been transported towards the front of the plot. Both Figure 4 and Figure 5 indicate that structures in the region of flow diagonally above the corner of the inner duct are stretched in the downstream direction.

The plots of isosurfaces of helicity density outline the turbulence structures in regions of the flow where the absolute value of the velocity vector is relatively high. This corresponds to locations where most of the transport of vorticity is taking place. However, the plots do not indicate where the structures are formed along the inner duct wall since the magnitude of the velocity vector is small in that region of flow.

Plots indicating isosurfaces of positive and negative values of the discriminant D are shown in Figures 6 and 7 for the same two instances in time: 39.175 and 39.230 non-dimensional time units into the large eddy simulation. The plots are oriented in the same manner, with the inner duct located in the bottom right corners. Regions of flow with positive values of D, *ie.* where the strain tensor is dominated by the rotation tensor, are associated turbulence structures described by vortex bundles. The discriminant plots do not exhibit the smooth isosurfaces that were observed in the helicity density plots. The shape of the vortex bundles can change significantly from one timestep to the next, although the general location of regions of pisitive D in the flow field remains relatively constant. This may be due, in part, to the coarse resolution of the large eddy simulation grid. Even though the shapes of the vortex bundles are not identical to those highlighted by the helicity density plots, regions of flow with a positive discriminant are associated with regions of high absolute helicity density. However, the reverse does not apply. In Figure 6, two large vortex bundles can be observed which correspond with regions of high absolute helicity density shown in Figure 4: at the front centre of the plot (Structure 1); and near the top left corner of the plot, mid-way along the x-axis (Structure 2). However, the structure observed mid-way along the x-axis in Figure 5 (Structure 3) does not appear in Figure 7. Investigation of additional topological parameters may be required to understand why this occurs.

The discriminant plots clearly show structures forming along the inner duct wall near the sharp corner. Figure 6 indicates a vortex bundle along the top of the inner duct wall (Structure 1) which separates from the wall at the corner, and then expands outwards diagonally towards the upper left corner of the plot. A different structure, Structure 2, shown at the front of Figure 7, is smaller and is attached to both walls close to, but not right at, the corner of the inner duct. It appears to be breaking up into smaller vortex bundles. Examination of data at later time points indicates that this does indeed occur, and the smaller vortex bundles are then transported downstream unattached to the inner duct. Vortex bundles at or near the corner of the inner duct were noted in all of the data examined between 39.0 and 39.5 non-dimensional time units into the large eddy simulation.

Information from the time-average secondary velocity, the helicity density, and the topology of the eddying motions can be combined to postulate how the presence of the sharp corner of the inner duct affects the development of turbulence structures in the flow field. The vorticies in the secondary velocity plot suck fluid towards the inner duct walls and accelerate it along the surface towards the sharp corner. Coherent structures consisting of vortex bundles form near the corner as the velocity of the secondary flow increases. At the corner, the flow is accelerated diagonally outwards, transport-

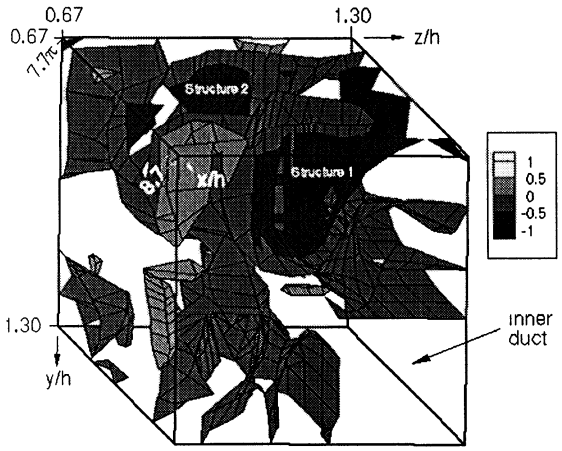

Figure 4: Helicity density at the top left corner of the inner duct at 39.175 non-dimenesional time units into the large eddy simulation

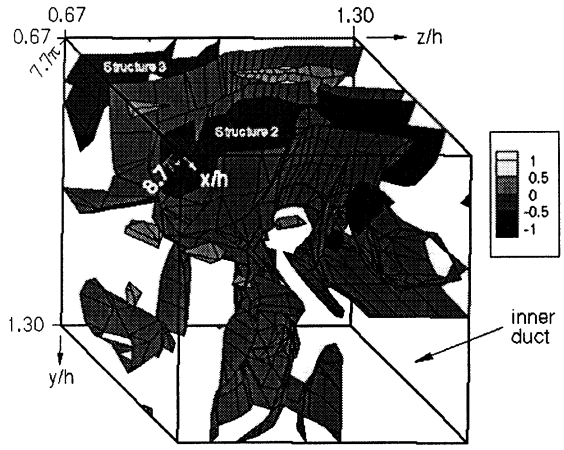

Figure 5: Helicity density at the top left corner of the inner duct at 39.230 non-dimenesional time units into the large eddy simulation

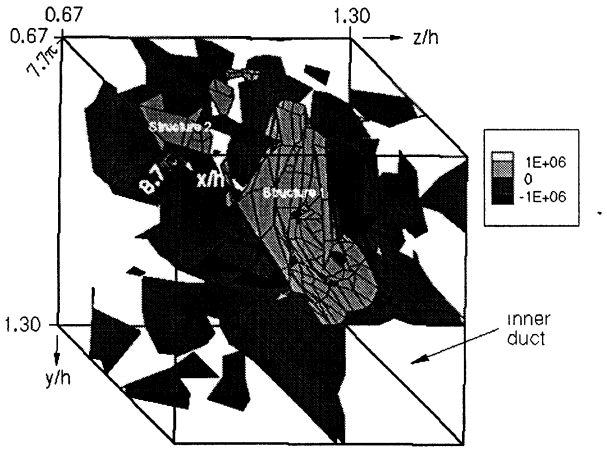

Figure 6: Isosurfaces of the discriminant D (see Equation 11) at the top left corner of the inner duct at 39.175 non-dimenesional time units into the large eddy simulation

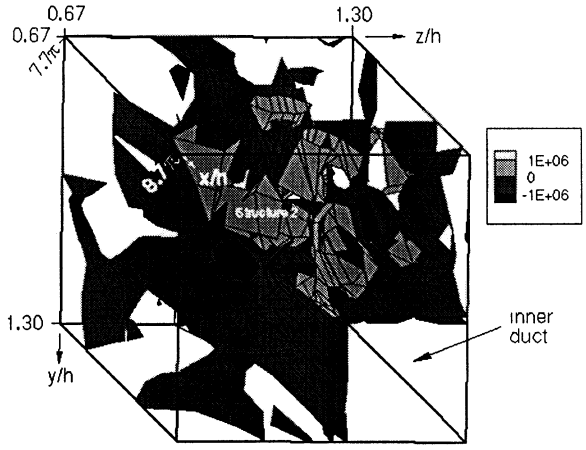

Figure 7: Isosurfaces of the discriminant D (see Equation 11) at the top left corner of the inner duct at 39.230 non-dimenesional time units into the large eddy simulation

ing the structures in this direction. As the structures reach into the mean velocity field, they are stretched downstream, creating a three-dimensional object. Occasionally, the structures separate from the inner duct and are transported downstream unattached.

To date, only the region of flow surrounding the inner duct corner has been analysed using flow topology techniques. Turbulence structures may also be formed in other regions of the flow, particularly near the corners of the outer duct, which will then interact with the structures observed in the present study.

4. CONCLUSIONS AND FUTURE WORK

The results presented here show that flow topology is a very useful tool for identifying the turbulence structures in a flow field from a numerical simulation. The combination of the helicity density and the discriminant isosurface plots, along with the time-averaged data of Xu and Pollard, provides an insight into the formation of turbulence structures in the square annular duct. Structures form near the inner duct corner, are transported diagonally outwards by the secondary flow field, and then stretched downstream by the mean flow field.

The work is ongoing and additional analysis of the data is required to fully understand the development of the turbulence structures. It is not clear why all of the structures outlined by isosurfaces of helicity density do not appear in the discriminant plots. Only the region of flow surrounding one inner duct corner has been examined. Turbulence structures formed elsewhere will interact with those observed here, affecting the entire flow field. Also, the use of the Smagorinsky subgrid scale model in the large eddy simulation database is expected to introduce errors in the observed shape of the turbulence structures. A dynamic subgrid scale model should improve the results. However, despite the limitations of the numerical database, the use of flow topology techniques has permitted the identification of clear and ordered turbulence structures contained in a flow field generated by a large eddy simulation.

REFERENCES

Blackburn, H.M., Mansour, N.N., and Cantwell, B.J., 1996, "Topology of fine-scale motions in turbulent channel flow," *Journal of Fluid Mechanics*, Vol. 310, pp. 269-292.

Chong, M.S., Soria, J., Perry, E.A., Chacin, J., Cantwell, B.J., and Na, Y., 1998, "Turbulence structures of wall-bounded shear flows found using DNS data," *Journal of Fluid Mechanics*, Vol. 357, pp. 225-247.

Chong, M.S., Perry, A.E., and Cantwell, B.J., 1990, "A general classification of three-dimensional flow fields," *Physics of Fluids*, Vol. A2, pp. 765 - 777.

Kim, J., and Moin, P., 1985, "Application of a Fractional-Step Method to Incompressible Navier-Stokes Equations," *Journal of Computational Physics*, Vol. 59, pp. 303-323.

Moffat, H.K., 1969, "The degree of knottedness of tangled vortex lines," *Journal of Fluid Mechanics*, Vol. 35, part 1, pp. 117-129.

Piomelli, U., 1993, "Applications of large eddy simulation in engineering: an overview," in *Large Eddy Simulation of Complex Engineering and Geophysical Flows*, B. Galperin and S.A. Orszag, eds. Cambridge University Press, Cambridge, pp. 119.

Xu, H.Y., and Pollard, A., 1997, "Large eddy simulation of annular duct flow using parallel computation," *Proceedings of the First AFOSR International Conference on DNS/LES*, C. Liu and Z. Liu, eds. Greyden Press, Columbus, OH, pp. 299-306.